Chengyu Liu¹ and Guanghui Hu^{1,2,3*}

¹Department of Mathematics, Faculty of Science and Technology, University of Macau, Macao SAR, China.. ²Zhuhai UM Science & Technology Research Institute, Zhuhai,

Guangdong, China...

³Guangdong-Hong Kong-Macao Joint Laboratory for

³Guangdong-Hong Kong-Macao Joint Laboratory for Data-Driven Fluid Mechanics and Engineering Applications, University of Macau, Macao SAR, China..

*Corresponding author(s). E-mail(s): garyhu@um.edu.mo; Contributing authors: cyliu3551@gmail.com;

Abstract

In a dual weighted residual method based on the finite element framework, the Galerkin orthogonality is an issue which prevents solving the dual equation in the same space to the one for the primal equation. In the literature, there have been two popular approaches to construct a new space for the dual problem, i.e., refining mesh grids (h-approach) and raising the order of approximate polynomials (p-approach). In this paper, a novel approach is proposed for the purpose based on the multiple-precision technique, i.e., the construction of the new finite element space is based on the same configuration to the one for the primal equation, except for the precision used for the finite arithmetic calculation in the computer. The feasibility of such a new approach is discussed in detail in the paper, from which it can be seen that the Galerkin orthogonality is avoided effectively. A main feature of our approach is that the remarkable improvement on both the efficiency and the storage can be expected compared with the h-approach and the p-approach, since necessary operations such as remeshing, regenerating finite elements and their integration environments in classical approaches can be avoided in the algorithm. Furthermore, with the generic programming feature template in C++, the proposed multipleprecision approach can be realized conveniently by using the precision

as a template parameter. A number of numerical examples successfully confirm the feature of our method, in which upto an order of magnitude improvement on the CPU time can even be observed in generating the error indicator, compared with classical h-approach and p-approach. It is worth mentioning that the performance of our approach is comparable with the one through a higher order interpolation (i-approach) in the literature. The combination of two approaches is believed a way to further enhancing the efficiency of the dual weighted residual method.

Keywords: finite element method; *h*-adaptive mesh method; dual-weighted residual; multiple-precision; C++ template

1 Introduction

Recently, the use of adjoint equations and duality arguments in residual-based a posteriori error estimation has become one of the most popular topics in the numerical analysis of partial differential equations. The idea can be traced back to the work of Babuška and Miller [1–3]. Then the techniques were systematically developed for more general situations [4–6]. Furthermore, Becker and Rannacher improved this approach into a computation-based feedback method, i.e. the dual weighted residual (DWR) method, which has the goal-orientation property [7–10]. Related techniques using duality arguments in post-processing and design have been studied in [11–14]. Due to the capability of dealing with the quantities of interest, the DWR method has been applied in many areas, such as mechanics, physics, and chemistry [15–21].

The idea of the DWR method can be described as follows. First of all, based on the finite element method, the Galerkin solution u_h is obtained from the finite element space $V_h \subset V$, where V is the variational space of the solution u. Then we introduce the target functional $J(\cdot)$, which can represent the quantity of interest based on u. The goal is to control the target error $J(u) - J(u_h)$. For simplicity, $J(\cdot)$ is assumed linear here. Following the general concept of the DWR method, by solving the dual problem associated with $J(\cdot)$, the dual solution z can be obtained. With the combination of $||u - u_h||$ and ||z||, we can get the so-called dual weighted residual error estimation of $|J(u) - J(u_h)|$. In simulations, $||u - u_h||$ can be evaluated by the classic a posteriori error estimation. Then finding the approximation \tilde{z} is the only left issue to deliver a quantized error estimation. It is noted that \tilde{z} needs to be calculated from a space different from V_h , due to the Galerkin Orthogonality $a(u - u_h, v) = 0$, $\forall v \in V_h$, which results in following classic approaches for generating \tilde{z} [9, 14, 15]:

• By h-approach: the new space is built on a mesh generated from refining the original mesh (using a finer mesh), from which \tilde{z} could be obtained.

- By p-approach: the new space is built by introducing more degrees of freedom into the original mesh (using a higher order finite element), from which \tilde{z} could be obtained.
- By *i*-approach: the approximation \tilde{z} is obtained by patch-wise higher-order interpolation of the numerical solution $z_h \in V_h$.

Although the above first two approaches are different with each other from the implementation point of view, they follow the same framework, i.e., a larger finite element space needs to be built first, then the dual problem will be discretized in this space, and the derived larger system of linear equations will be solved for the dual solution. In the above framework, several operations would be necessary, i.e., re-meshing, re-organizing the degrees of freedom, regeneration of the information of numerical quadrature, reformation of stiff matrix, and solving an even much larger system of linear equations. Consequently, nonignorable computational resources are occupied in the simulation by these two approaches. As for the higher-order interpolation approach, the reliable approximation \tilde{z} is obtained through the patch-wise interpolation operation to break the Galerkin orthogonality. In this work, different from the idea of the above classic approaches, we explore the possibility of building a different finite element space for solving the dual problem through one feature of the computer, i.e., finite precision arithmetic.

A key observation is that when the finite element space V_h is expressed in different floating point precision formats, they should be two different finite element spaces from the computer point of view, even both spaces are built with the same configuration (same mesh, degrees of freedom, basis functions, etc). To understand it, we need to recall the way a real number is expressed in the computer. It is known that from IEEE standard shown in Fig. 1.1, each real number takes up 64 bits in double-precision formats, 32 bits in float-precision formats, and 16 bits in half-precision, respectively. Consequently, one number stored with different precision formats will be treated as different numbers in calculations.

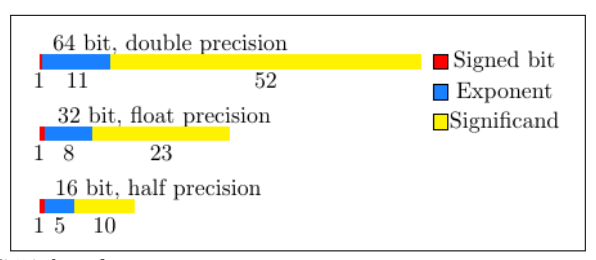


Fig. 1.1 IEEE754 data format.

Hence, if we take two vectors $\vec{v}_1 = (\cos\frac{\pi}{3}, \sin\frac{\pi}{3})$ and $\vec{v}_2 = (-\sin\frac{\pi}{3}, \cos\frac{\pi}{3})$ as an example, it can be seen that two vectors are orthogonal with each other mathematically. Numerically, if two vectors are expressed in single-precision, the inner product (\vec{v}_1, \vec{v}_2) is computed as 0.00000000. However, if \vec{v}_1 is in single,

and \vec{v}_2 is in double, then the inner product becomes -0.000000007771812, which is obviously not zero in double-precision. Such an observation motivates an idea for the implementation of DWR, i.e., solving primal and dual problems in two different precision formats to avoid the Galerkin orthogonality.

In this paper, a multiple-precision DWR (MP-DWR) method is proposed for the implementation of h-adaptive finite element methods, towards improving the simulation efficiency. The flowchart of the method can be summarized as follows. First of all, let V_h^d denotes the finite element space built on the partition \mathcal{T} of the domain Ω in double-precision, on which numerical solution u_h^d and corresponding error estimation are obtained. Then a new finite element space V_h^f is built on the same partition \mathcal{T} in float-precision, on which the dual solution z_h^f is obtained. Based on these, a DWR a posteriori error estimation can be generated to serve the following local refinement of the mesh grids in the h-adaptive mesh method. The feasibility of above algorithm is discussed in detail in the paper, from which the break of the Galerkin orthogonality can be seen clearly in examples.

The improvement for the efficiency can be expected from our method by observations that i). both the re-partitioning of mesh grids and the rearrangement of degree of freedoms as well as associate basis functions are avoided in our method, as a comparison, h- and p-approach both need these operations for solving the dual problem in implementations, and ii). the involvement of single-precision calculation would bring the reduction of both CPU time and storage. In numerical experiments, the significant acceleration by our method can be seen clearly, e.g., in solving 3D Poisson equation, around an order of magnitude difference of CPU time between the h-approach strategy and our method can be observed in the generation of the error indicator.

Another feature of our MP-DWR method is its concise coding work with the aid of template property in C++ language. In this paper, all simulations are realized by using a C++ library AFEPack[22], in which the code is organized following a standard procedure on solving partial differential equations, i.e., partitioning the domain, building a finite element space, forming a system of linear equations, imposing boundary conditions, as well as solving the system of linear equations. More importantly, each step in above procedure is realized as a module in AFEPack. Consequently, using the feature template of the C++ language and using the type of the floating-point number as a parameter of the template class would be a perfect choice for coding the MP-DWR method, which makes the code concise and easily managed.

The outline of this paper is as follows: In Section 2, based on the Poisson equation, the idea of goal-orientation and the dual weighted residual method in h-adaptive finite element methods are briefly reviewed. In Section 3, we describe a novel DWR implementation based on multiple-precision in detail. In Section 4, several numerical experiments are implemented, in which the validity and acceleration of the proposed method can be demonstrated. Besides that, the capability of the proposed method for solving the eigenvalue problem is also shown. In addition, several remarks are delivered about the properties

and limitations of the proposed method, based on our numerical experience. Finally, we give the conclusion of this paper and future works in Section 5.

2 Poisson equation and DWR based h-adaptive mesh methods

In this section, based on the Poisson equation, a DWR based h-adaptive finite element method is reviewed briefly, as well as the associated classic theory.

2.1 Poisson equation and finite element discretization

Consider the Poisson equation

$$\begin{cases}
-\Delta u = f, & \text{in } \Omega, \\
u = 0, & \text{on } \partial\Omega,
\end{cases}$$
(1)

where the unknown u and f are two functions defined on the domain Ω , and we consider a homogeneous Dirichlet boundary condition on the boundary $\partial\Omega$ for the well posedness. $\Omega\subset\mathbb{R}^d$ is a bounded domain in two (d=2) or three (d=3) dimensional space. We choose the variational space $V=H^1_0(\Omega)$ to incorporate the homogeneous Dirichlet boundary condition. The inner product of V is defined as

$$(u,v) = \int_{\Omega} uv d\vec{x}.$$
 (2)

Then integration by parts yields the bilinear operator $a(\cdot,\cdot)$:

$$(f,v) := \int_{\Omega} fv d\vec{x} = \int_{\Omega} (-\Delta u)v d\vec{x}$$

$$= \int_{\Omega} \nabla u \cdot \nabla v d\vec{x} - \int_{\partial \Omega} v \frac{\partial u}{\partial \vec{n}} ds$$

$$= \int_{\Omega} \nabla u \cdot \nabla v d\vec{x} := a(u,v),$$
(3)

where \vec{n} denotes the outward unit normal to $\partial\Omega$. The weak solution u to the Poisson equation can be characterized via the variational problem:

Find
$$u \in V$$
, such that $a(u, v) = (f, v), \forall v \in V$. (4)

Based on the triangulation \mathcal{T} , we can introduce the finite element space $V_h \subset H_0^1(\Omega)$. In V_h , the Ritz-Galerkin approximation to (4) can be expressed as:

Find
$$u_h \in V_h$$
, such that $a(u_h, v) = (f, v), \forall v \in V_h \subset V,$ (5)

where u_h is the Galerkin approximation to u.

2.2 Goal-orientation and dual weighted residual

In this subsection, the classic residual type a posteriori error estimation is introduced first, then an introduction of the framework of a goal-oriented a posteriori error estimation based on DWR method follows.

Denote the exact solution of (1) and (5) by u and u_h , respectively. Generally, the exact form of u is unknown so it is impossible to compute the error $e_h := u - u_h$. However, the error e_h is related to the residual as:

$$a(e_{h}, v) = a(u - u_{h}, v)$$

$$= \int_{\bar{\Omega}} \nabla(u - u_{h}) \cdot \nabla v d\vec{x}$$

$$= \int_{\Omega} fv + \int_{\Omega} \nabla u_{h} \cdot \nabla v d\vec{x} = \mathcal{R}(v), \quad \forall v \in V.$$
(6)

Then integration by parts element-wise to transform \mathcal{R} as:

$$\mathcal{R}(v) = \sum_{K} \int_{K} (f + \Delta u_h) v d\vec{x} + \sum_{E} \int_{E} r[\vec{n}_e \cdot \nabla u_h] v ds, \tag{7}$$

where K and E represent elements and the edges of elements, respectively. For any piecewise continuous function v and any interior edge E, the "jump" term r of v across E in the direction of \vec{n}_E is defined as in [23]:

$$r(v)(x) = \lim_{t \to 0^+} v(x - t\vec{n}_E) - \lim_{t \to 0^+} v(x + t\vec{n}_E), \forall x \in E.$$
 (8)

Based on (7), a classic residual-based error indicator for every element $K \in mesh \mathcal{T}$ can be obtained as

$$\eta_K^{resi} = \left\{ h_K^2 \| \bar{f}_K + \Delta u_h \|_K^2 + \frac{1}{2} \sum_{E \in \varepsilon_{K,\Omega}} h_E \| r(\vec{n} \cdot \nabla u_h) \|_E^2 \right\}^{\frac{1}{2}}, \tag{9}$$

where $\varepsilon_{K,\Omega}$ represents the set which contains all interior boundaries of element K, and f represents the average of f on element E. What is more, there are two constants c^* and c_* , which only depend on the shape parameter of T, such that the estimates

$$\|\nabla(u - u_h)\| \le c^* \{ \sum_{K \in \mathcal{T}} (\eta_K^{resi})^2 + \sum_{K \in \mathcal{T}} h_K^2 \|f - \bar{f}_K\|_K^2 \}^{\frac{1}{2}}$$
 (10)

and

$$\eta_K^{resi} \le c_* \{ \|\nabla(u - u_h)\|_{\omega_K}^2 + \sum_{K' \subset \omega_K} h_{K'}^2 \|f - \bar{f}_{K'}\|_{K'}^2 \}^{\frac{1}{2}}$$
 (11)

hold for all elements $K \in T$. ω_K is defined as:

$$\omega_K = \bigcup_{\varepsilon_K \cap \varepsilon_{K'} \neq \emptyset} K', \tag{12}$$

where ε_K represents the set which contains all boundaries of element. Consequently, the bound of error $e = u - u_h$ can be obtained as [23, 24]:

$$C_2(\sum_K (\eta_K^{resi})^2)^{\frac{1}{2}} \le \|\nabla(u - u_h)\| \le C_1(\sum_K (\eta_K^{resi})^2)^{\frac{1}{2}}.$$
 (13)

Combining (9)-(13), the error can be evaluated by using such an *a posteriori* error indicator based on the residual \mathcal{R} , which is computable from f and u_h . With the help of the *a posteriori* error indicator, the mesh can be refined to capture the critical regions of the exact solution. On such an adapted mesh, numerical simulations could be implemented more efficiently.

Generally, in practical numerical simulations, the quantities of interest can be some functionals of the exact solution u. But the classic residual-based estimates mainly focus on the energy norm or L^2 norm of the problems. These norms are usually different from the quantities of interest. Thus, the classic residual-based error estimates are not a good choice for the adaptation strategy anymore. To fix this, we consider the goal-orientation adaptation strategy, in which some terms consisting of goals, i.e. quantities of interest, should be added to the error estimates.

The dual weighted residual method is one class of goal-orientation adaptation approaches, which can be briefly summarized as follows. Following by [10, 15], we still consider the Poisson equation (1) with the finite element discretization as above. Assume $J(\cdot)$ is the target functional which is linear. And $J(\cdot)$ satisfies

$$a(v,z) = J(v), \quad \forall v \in V,$$
 (14)

where $z \in V$ is the solution of the associated dual problem. With $\varphi_h \in V_h$, (14) can be represented as

$$a(\varphi_h, z_h) = J(\varphi_h), \quad \forall \varphi_h \in V_h,$$
 (15)

where $z_h \in V_h$. Combining (14) and (15), we can get the target functional of e:

$$J(e) := J(u - u_h) = a(u - u_h, z).$$
(16)

To get the refinement indicator, we can compute the cell-wise integration by parts:

$$J(u) - J(u_h) = J(e) = \sum_{K \in \mathcal{T}_h} \{ (R_h, z)_K + \frac{1}{2} (r(\vec{n} \cdot \nabla u_h), z)_{\partial K} \}$$

=: η , (17)

where the cell residual R_h is defined by

$$R_{h|K} := f + \Delta u_h. \tag{18}$$

In simulations, with the approximation $\tilde{\eta}$ to η , the effectivity of the error indicator can be evaluated through the index given by

$$I_{eff} = \left| \frac{\tilde{\eta}}{J(e)} \right|,\tag{19}$$

which represents the degree of overestimation and should desirably be close to one [15]. Moreover, a posterori error estimate can be obtained as

$$|J(e)| \le \eta_{\omega} := \sum_{K \in \mathcal{T}_b} \rho_K \omega_K, \tag{20}$$

where the cell residuals ρ_K and weights ω_K are given by:

$$\rho_K := (\|R_h\|_K^2 + \frac{1}{2}h_K^{-1}\|r(\vec{n} \cdot \nabla u_h)\|_{\partial K}^2)^{1/2},
\omega_K := (\|z\|_K^2 + h_K\|z\|_{\partial K}^2)^{1/2}.$$
(21)

Such an error estimation consists of the numerical primal solution and the exact dual solution. The product of $\|\rho_K\| \|\omega_K\|$ is the so-called dual weighted residual, in which $\|\rho_K\|$ evaluate the residual of the primal solution and $\|\omega_K\|$ is the weight given by the dual solution z. In the calculations of building the dual weighted residual indicator, the term associated with ρ_K can be computed based on the primal solution. But the exact dual solution z is generally unknown. Then the only left issue is to obtain the approximation \tilde{z} . It should be noticed that the approximation \tilde{z} can not be computed in the same space V_h as the one for solving the primal problem otherwise the error indicator would be a trivial value due to Galerkin orthogonality:

$$a(u - u_h, v_h) = 0, \ \forall v_h \in V_h. \tag{22}$$

In the process of computing the approximation \tilde{z} , suppose the numerical primal solution u_h has been computed from the space V_h on the mesh \mathcal{T}_h . Based on these, there are three main classic approaches for computing \tilde{z} as follows.

• By h-approach: A denser mesh $\tilde{\mathcal{T}}_h$ can be constructed by globally refining the mesh \mathcal{T}_h . Based on $\tilde{\mathcal{T}}_h$, a different space \tilde{V}_h can be built. Then the dual solution \tilde{z} can be obtained from V_h , e.g.,

Find
$$\tilde{z} \in \tilde{V}_h$$
, whose mesh size is smaller than h. (23)

• By p-approach: A finite element space $\tilde{V}_h^{(2)}$ with quadratic (or higher-order) finite elements has to be constructed. From $\tilde{V}_h^{(2)}$, the dual solution \tilde{z} can be obtained, e.g.,

Find
$$\tilde{z} \in \tilde{V}_h^{(2)}$$
, whose polynomial order is higher than V_h . (24)

• By *i*-approach: The bilinear Ritz projection $z_h \in V_h$ of z is computed first. Then the approximation \tilde{z} is obtained by patch-wise higher-order interpolation of z_h . In the following numerical experiments, we only consider *quadratic* interpolation.

Remark 1 In numerical simulations, we only use the triangle element (for 2-D) and tetrahedron element (for 3-D), which makes the interpolation operation quite different from cases with rectangle and hexahedron elements. To achieve the interpolation, we construct the patch-wise of one element based on all its neighbors. By solving a least-square problem, we can get the high-order interpolation of z in the corresponding element.

In practical simulations, the first two approaches all build a different finite element space for solving the dual problem. In such a process, some operations would be necessary, i.e., remeshing the grid, re-organizing the degree of freedoms, regeneration of the information of numerical quadrature, the reformation of a larger scale stiff matrix, and solving an even larger linear system of linear equations. These operations would cost nonignorable CPU time and memory storage in calculations. To avoid these steps, the i-approach obtains the approximation \tilde{z} by using higher-order interpolation, which makes it cheaper than the other two classic approaches [20]. Different from three classic approaches above, we expect to propose a novel approach to avoid the Galerkin orthogonality. Such a new approach can also avoid these operations so the acceleration in simulations can be expected.

3 A novel DWR implementation based on multiple-precision

In the introduction, we give an example to show that: With the help of multiple-precision, orthogonality of two vectors can not be preserved numerically. In this section, based on the same idea, we introduce a new implementation of DWR, in which the multiple-precision will be used to effectively break the Galerkin orthogonality.

As mentioned above, the two classic approaches (23) and (24) both have to implement several operations to build a different finite element space for the dual problem, by which nonignorable computational resources are occupied. Therefore, we naturally want to avoid these operations in our implementation to speed up computations. To achieve this point, multiple-precision is a possible

option. Next, we will first show how the multiple-precision breaks the Galerkin orthogonality to make sure this idea works.

Firstly, the Galerkin orthogonality in (22) indicates that: for $v_h = u_h$, we have

$$a(u - u_h, u_h) = 0. (25)$$

Then we will show that (25) will not be held with solutions from different precision formats. By using a different precision format, a different space V'_h can be built on computers without changing the mesh grid. In V'_h , the numerical solution u'_h can be obtained. Based on the above idea, u_h and u'_h would be different since they are computed with different precision formats. Furthermore, they are obtained from two different finite element spaces V_h and V'_h , respectively. Thus, it can be expected that the Galerkin orthogonality between them would not be preserved:

$$a(u - u_h, u_h') \neq 0. \tag{26}$$

Based on this, we implement several numerical experiments with multiple-precision. In the following two examples, multiple-precision is implemented by using a combination of double- and float-precision.

Here, we only focus on the Poisson equation in 2-dimensional with the exact function as $u=\sin(\pi x)\sin(2\pi y)$ and in the domain $\Omega=(-1,1)^2$. To compute the numerical solution u_h of the Poisson equation, the finite element space V_h^d is built firstly. In V_h^d , a numerical result u_h^d can be obtained. Then the similar operations are implemented in float precision, we can obtain the numerical solution u_h^f from V_h^f . With these two numerical solutions, we can compute the value of $a(u-u_h^d,u_h^d)$ and $a(u-u_h^d,u_h^f)$ to check if (22) and (26) hold. The numerical results are shown in Table 3.1. To test the solution with singularity in the domain, we change the exact solution as $u=50(1-x^2)(1-y^2)exp(1-y^{-4})$. Then we repeat the operations as above to obtain the numerical solutions u_h^d and u_h^f . The corresponding numerical results are shown in Table 3.2.

Dofs	L2 Error	$a(u-u_h^d, u_h^d)$	$a(u-u_h^d, u_h^f)$
385	4.470e-1	-5.035e-5	-8.117e-5
$1473 \\ 5761$	1.136e-1 2.854e-2	-1.579e-7 -6.596e-10	-5.103e-4 -2.202e-3
22785	7.143e-3	8.254 e-11	-9.337e-3

Table 3.1 Galerkin orthogonality of u_h^d and u_h^f for the case $u = sin(\pi x)sin(2\pi y)$.

Tables 1 and 2 show that the error in L2-norm (L2 Error) tends to zero as refining the mesh, such that the numerical solution u_h^d and u_h^f get more accurate with more Dofs (degrees of freedom). Meanwhile, the value of $a(u-u_h^d,u_h^d)$ tends to zero, which means the Galerkin orthogonality of u_h^d is numerically preserved better. That is the reason that we can not directly compute the dual solution in the same space with the same precision to build the DWR error indicator in numerical experiments. On the contrary, the value of

Dofs	L2 Error	$a(u-u_h^d, u_h^d)$	$a(u-u_h^d, u_h^f)$
385	4.879e-2	-1.039e-8	-2.483e-6
1473	1.234e-2	-4.164e-11	-9.306e-6
5761	3.094e-3	6.610e-13	-5.054e-5
22785	7.742e-4	4.830e-13	-1.938e-4

Table 3.2 Galerkin orthogonality of u_h^d and u_h^f for the case $u=50(1-x^2)(1-y^2)exp(1-y^{-4})$.

 $a(u-u_h^d,u_h^f)$ gets further away from zero as the number of Dofs increases, which means the Galerkin orthogonality between u_h^d and u_h^f is numerically broken more obviously. Based on this phenomenon, we can confirm that the Galerkin orthogonality between u_h^d and u_h^f can be numerically broken by multiple-precision.

From the above discussion, the Galerkin orthogonality can be avoided by solving primal and dual problems in two different precision formats. Thus, it can be expected that dual solutions from the finite element space constructed with different precision will work in the DWR method. With such primal and dual solutions, a reliable DWR error indicator can be obtained for mesh adaptation. Based on this, we propose Algorithm 1 for the multiple-precision implementation of the DWR method.

Algorithm 1 Framework of Adaptive finite element method based on MP-DWR(DF) method.

Require: The initial mesh, \mathcal{T}_0 ; The tolerance, tol; The maximum iteration times, Max_{iter} ; the iteration times k = 0.

- 1: Build a finite element space V_h on the mesh \mathcal{T}_k ;
- 2: Solve the primal problem in double-precision to get the primal solution u_h^d ;
- 3: Solve the dual problem in float-precision to get the dual solution z_h^f ;
- 4: Calculate the cell residual $\tilde{\rho}_K$ and weights $\tilde{\omega}_K$ for each element to construct the error indicator $\tilde{\eta}_{\omega}$ as (20);
- 5: Check the stopping condition: If $\tilde{\eta} < tol$ or $k > Max_{iter}$, stop the adaptation and return the numerical solutions.
- 6: Else, adapt the current mesh with $\tilde{\eta}_{\omega}$ to get the new mesh \mathcal{T}_{k+1} , update the iteration times k = k + 1 and return to step 1.

Remark 2 In the above framework of MP-DWR(\mathbf{DF}) method, the primal problem is solved in \mathbf{D} ouble-precision. As for dual problem, it is solved with \mathbf{F} loat-precision. In fact, the framework of MP-DWR(FD) is also useful, i.e. solving the primal and dual problem in Float and Double precision, respectively. But there are some limits of MP-DWR(FD), which will be shown through a numerical example (4.4) in the following part. So in this paper, MP-DWR(DF) framework is used by default in numerical experiments if not specified.

Such a new implementation of DWR method has a series of advantages, which can be summarized as follows:

First of all, several repeated operations of building finite element space can be avoided. Compared to the two classic methods (h-approach and p-approach), the MP-DWR method only computes the modules of building the finite element space once in one iteration. With the help of multiple-precision, the re-partitioning of the mesh grid, the rearrangement of degrees of freedom, the recalculation of the quadrature information, the reformation of stiff matrix, and solving an even larger linear system of linear equations can be avoided in the process of obtaining the dual solution. Without these operations, considerable improvements in efficiency can be obtained.

As for the i-approach, although it can avoid these repeated options, the higher-order interpolation step is required to construct the error indicator. While MP-DWR method can directly use the dual solution from a different precision to generate the error indicator without such an interpolation operation. Thus, although the i-approach can obtain a more accurate dual solution compared to the MP-DWR method, it still can be expected that the MP-DWR method is faster than the i-approach in the implementation.

The second advantage of MP-DWR comes from the involvement of computations with low precision. On computers, if one number is stored in double-precision, it will cost 8 bytes. While it costs 4 bytes in single-precision. Thus, when a quantity of data is stored on computers in single-precision instead of double-precision, the storage memory will be saved by fifty percent. Besides that, data with lower precision is more conducive to accelerating the calculation. Consider following C++ codes:

```
double double_data = 0.;
for(int i = 0;i < 1.0e7;i ++)
{double_data += 4.0*atan(1.0);}
float float_data = 0.;
for(int i = 0;i < 1.0e7;i ++)
{float_data += float(4.0*atan(1.0));}</pre>
```

The same operation of the data is implemented 1.0e7 times with different precision formats. The corresponding CPU times for the calculations of the above two modules are recorded in Table 3.3. It is obvious that the CPU time for the calculations in float-precision is much less than double-precision. Above all, it can be expected that the calculations with single-precision can save memory storage and CPU time compared with double-precision. Therefore, the single-precision calculation part in the MP-DWR method can bring further reduction in both CPU time and storage.

In addition, the realization of the MP-DWR method can be very concise by using *template*. Templates are a feature of the C++ programming language that allows functions and classes to work on many different data types without rewriting the code for each one. In this paper, we implement all simulations

Table 3.3 CPU time for different precision

Precision format	CPU seconds
double	4.010e-2
float	2.448e-2

based on the AFEPack library [22]. The code in the AFEPack library follows a standard procedure for solving partial differential equations. Furthermore, each step in the standard produce of implementing finite element method is realized as a module based on template in AFEPack. So it is quite trivial to utilize the modules to realize Algorithm 1. The multiple-precision computations can be implemented by using the type of floating-point numbers as parameters of the modules. For example, consider the definition of the bilinear operator module in AFEPack:

By merely changing the *template* parameter 'Number' in the definition, we can easily change the precision of the numbers in *BilinearOperator*. Such a property of the *AFEPack* makes it convenient for us to build finite element spaces with different precision formats. By merely changing some parameters of the *template* class in modules, multiple-precision calculations can be implemented without repeating the entire code for each precision format, which makes the realization of codes for our method very concise. Moreover, the use of *template* also facilitates the modification of our codes based on some function libraries, which will help us to generate a practical package in the future. Codes of one numerical example of the MP-DWR method can be found in Github [25].

4 Numerical experiments

In this section, a series of examples are shown to demonstrate the validity and acceleration of the MP-DWR method. In the following numerical experiments, we use the linear triangle template element for 2D cases and the tetrahedron template element for 3D cases, respectively. All numerical examples presented in this paper are developed by using the AFEPack[22] in C++, and the hardware is a DELL Precision T5610 workstation with 12 CPU Cores, 3.6GHz and 64 Gigabytes memory.

Moreover, a high order Gaussian quadrature is recommended in the calculations since it can produce more accurate results, which can break the Galerkin orthogonality more obviously. Therefore, the MP-DWR error indicators can be more effective. Here, we use the six-order Gaussian quadrature in all computations.

4.1 Effectiveness of MP-DWR method

In this part, we conduct a series of numerical experiment based on MP-DWR method to verify its effectiveness. In the beginning, Poisson equation with special target functional is considered for testing the goal-orientation property of MP-DWR method. Then experiments of a problem with diffusion coefficient and the convection-diffusion equation are also conducted, respectively, to study whether the MP-DWR method can be effective in some more complex situations.

4.1.1 Poisson equation

In the beginning, we consider the Poisson problem:

$$\begin{cases}
-\Delta u = f, & \text{in } \Omega, \\
u = 0, & \text{on } \partial\Omega,
\end{cases}$$
(27)

where $\Omega = (-1,1) \times (-1,1)$. First of all, we study the effectivity indices of the MP-DWR method for different target functionals in the Poisson case. As a benchmark example in [15], we consider this Poisson problem (27) for an exact solution $u_1 = (1-x_1^2)(1-x_2^2)sin(4x_1)sin(4x_2)$ (as shown in Figure 4.1.1) with the target functionals:

$$J_{\text{area}}(u) := |S|^{-1} \int_{S} u d\vec{x}, \ S := \left[-\frac{1}{2}, 0 \right] \times \left[0, \frac{1}{2} \right], \ \vec{x} = (x_1, x_2),$$
$$J_p(u) := u(\vec{x}_e), \ \vec{x}_e = \left(\frac{1}{2}, \frac{1}{2} \right).$$
(28)

To evaluate the error indicator generated by MP-DWR, we compute the effectivity index I_{eff} given in (19). In Figure 4.1.2 we present effect indices of the MP-DWR approach applied to this Poisson case. It can be seen that effectivity indices of target functionals J_1 and J_p get closer to one as the number of Dofs increases. Although they are not strictly equal to one, they tend to around one. Therefore, we can confirm the effectivity of the MP-DWR method.

Then, a sharper function is considered, of which the exact form is given as $u_2 = 5.0 \times (1 - x_1^2)(1 - x_2^2)exp(1 - x_2^{-4})$. Besides that, we consider a point-wise output functional, which is given by:

$$J_p(u) := u(\vec{x}_e), \ \vec{x}_e = (0.2, 0.8).$$
 (29)

The numerical dual solution computed is shown as the right one in Figure 4.1.3. And the residual-based method with indicator η_K^{resi} as (9) is implemented for comparison. The refined mesh and numerical results are shown in Figure 4.1.4.

From the left two pictures in Figure 4.1.4, the adapted mesh based on residual based error indicator gets denser around the singularity of function u in the whole domain. By contrast, the adapted mesh based on MP-DWR method not only gets denser around the singularity but also adds much more degrees of freedom around the interested point. As a result, the MP-DWR

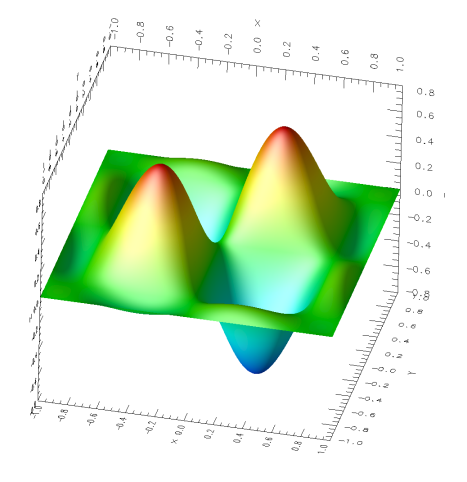


Fig. 4.1.1 The exact solution of u_1 .

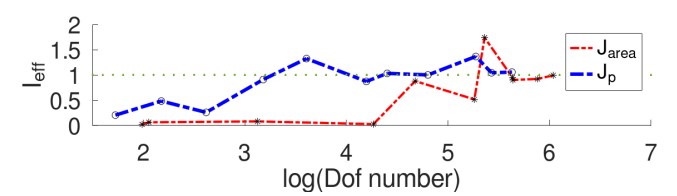


Fig. 4.1.2 Effectivity indices of MP-DWR error indicators for the target functionals J_{area} and J_p over the number of Dofs.

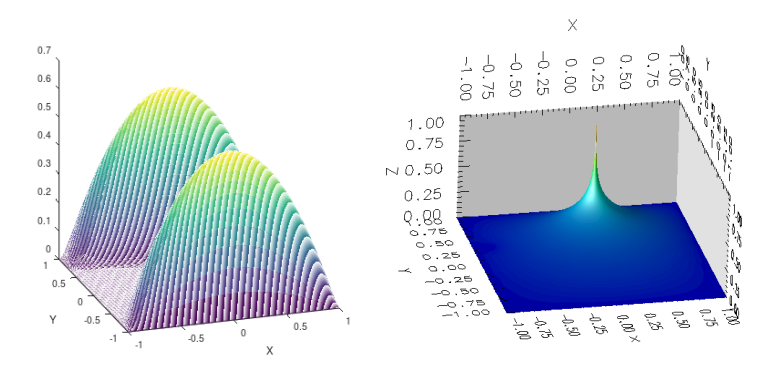
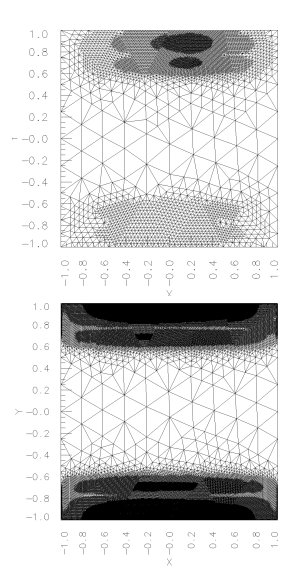


Fig. 4.1.3 Exact solution u_2 and corresponding dual solution.

method can deal with the point-wise target functional more precisely and economically. Moreover, the right picture in Figure 4.1.4 shows that the MP-DWR can obtain the numerical result reaching at the specified level with much more fewer degrees of freedom compared to the residual-based method. These phenomena confirm the goal-orientation property of the MP-DWR method,



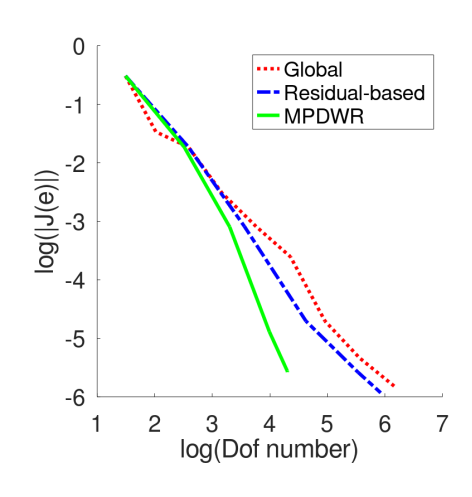


Fig. 4.1.4 Upper left: the adapted mesh based on MP-DWR. Lower left: the adapted mesh based on residual-based method. Right: the relationship between error in target functionals and degrees of freedom.

which also demonstrates the effectiveness of the MP-DWR method on the Poisson problem with some particular target functionals somehow.

Moreover, we also implement the h-approach, p-approach and i-approach for comparisons. The numerical results are shown in Figure 4.1.5. It can observed that the MP-DWR method can obtain a result of similar accuracy with a similar number of Dof compared to the three classic approach. Consequently, the efficiency of the MP-DWR method is comparable with the three approaches. However, the implementation of the MP-DWR method is faster, which makes the MP-DWR competitive. Such an advantage of the MP-DWR method will be shown in the following numerical example 4.2.

4.1.2 Coefficient elliptic equation

Before demonstrating the acceleration capability of the new method, we implement the MP-DWR method to some complex cases to check if it can still work in those situations. Here, we use a coefficient elliptic equation, which is given by

$$\begin{cases}
-\nabla A \nabla u_3 + c u_3 = f,, \text{ in } \Omega, \\
u_3|_{\partial\Omega} = 0,
\end{cases}$$
(30)

where A = aI with

$$a = \begin{cases} 10, \ x_1^2 - x_2^2 \le 0, \\ 1, \ x_1^2 - x_2^2 < 0. \end{cases}$$
 (31)

And we set c = 1 and f = 1. The figure of u_3 is shown in Figure 4.1.6. The

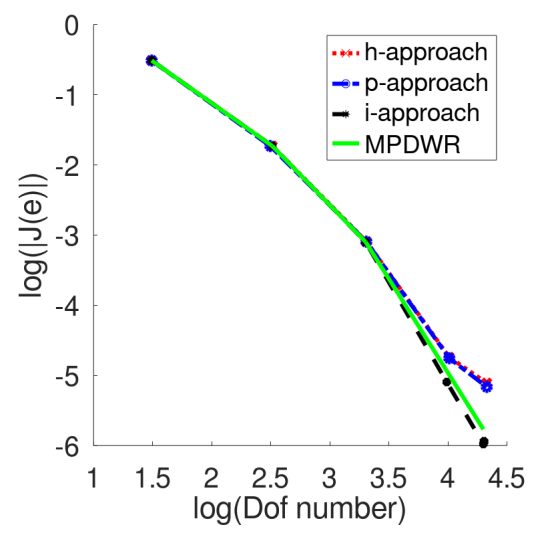


Fig. 4.1.5 The target error over the number of Dofs.

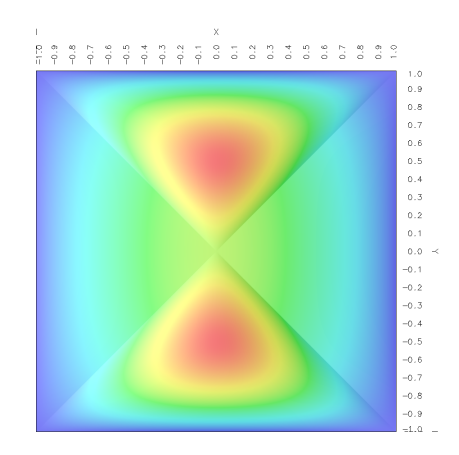


Fig. 4.1.6 The numerical solution of the function u_3 .

output functional of this case is defined by

$$J_p(u) := u(\vec{x}_e), \ \vec{x}_e = (0.5, 0).$$
 (32)

The bilinear form of this equation should also be changed. More details can be found in [22]. Based on that, an error indicator similar to (20) can be obtained. We implement the MP-DWR method and residual-based method to refine the mesh grid, respectively. The right picture in Figure 4.1.7 shows that target error over the number of Dofs. Since the mesh is too coarse in the beginning, slight oscillation can be observed. However, with the refinement of the mesh

grid, the convergence becomes smooth. Then it can be observed that the MP-DWR method can obtain the numerical result reaching the specified level with much fewer Dofs than the residual-based method. Besides that, from two left pictures in Figure 4.1.7, we can observe that the refined mesh based on MP-DWR can capture the goal point better. While the residual-based method provides a mesh, on which the solution can be approximated well in the whole domain. As a result, it has to cost more expensive numerical effort than the MP-DWR method to get accurate quantities of interest. Based on these, the effectiveness of the MP-DWR method in the coefficient elliptic equation can be verified.

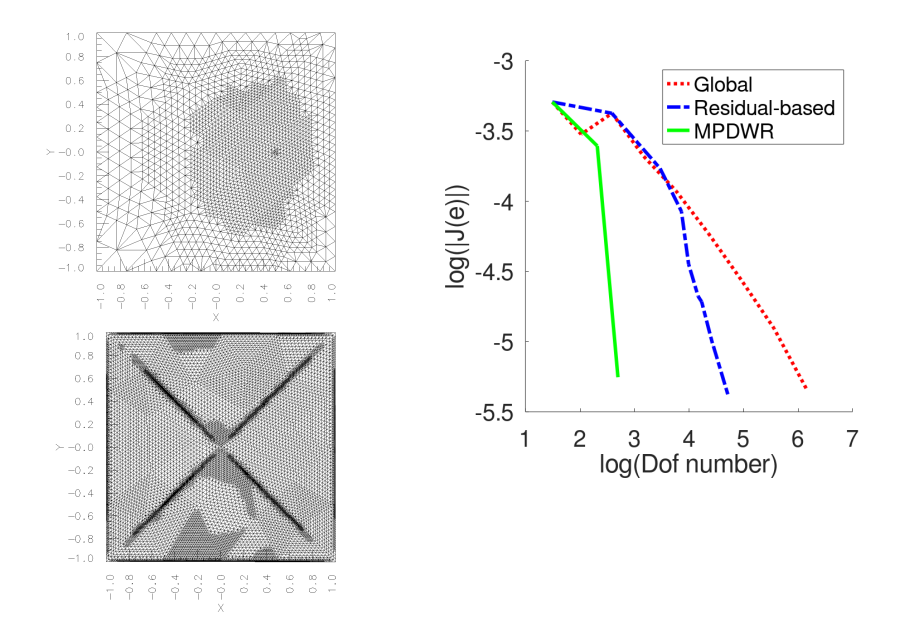


Fig. 4.1.7 Left: the adapted mesh based on MP-DWR. Middle: the adapted mesh based on residual-based method. Right: the log value of target functionals.

4.1.3 Convection-diffusion equation

To test the validity of MP-DWR method in other complex cases, we consider the convection-diffusion equation, which is given by

$$\begin{cases}
-\nabla \cdot (\epsilon \nabla) u + \vec{\alpha} \nabla u = f, & \text{in } \Omega, \\
u = 0, & \text{on } \partial \Omega,
\end{cases}$$
(33)

and the exact solution u is given as $u_4 = sin(2\pi x_1)sin(\pi x_2)$. In the numerical simulation, the ϵ is set as 0.01 and $\vec{\alpha} = [1, 1]$. Following Appendix A, we can get the error indicator for mesh adaptation. For comparison, residual-based

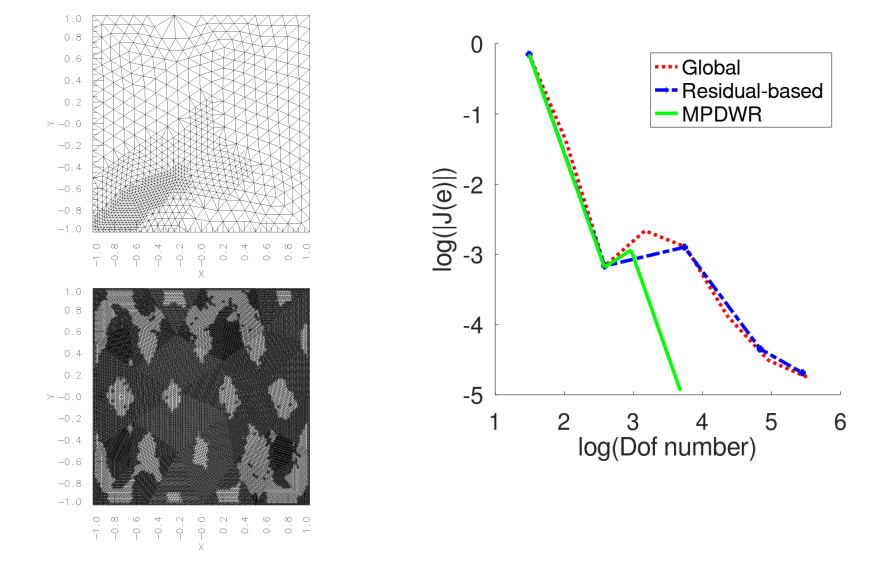


Fig. 4.1.8 Upper left: the adapted mesh based on the MP-DWR method. Lower left: the adapted mesh based on the residual-based method. Right: the relationship between error in target functionals and degrees of freedom.

method with η_K^{resi} is implemented in the simulation. In this case, the target functional is defined as the point-wise one:

$$J_p(u) := u(\vec{x}_e), \ \vec{x}_e = (-\frac{1}{3}, -\frac{1}{2}).$$
 (34)

Numerical results are shown in the Figure 4.1.8. This case nicely shows the goal-orientation property of MP-DWR method. It can be seen that the MP-DWR method sets more degrees of freedom around the interested point and along those finite elements that influence the error of interested point in the direction of the flow field $\vec{\alpha}$. As a comparison, the residual-based method puts more degrees of freedom on the whole domain. Consequently, the adapted mesh grids would be quite dense as the lower left picture in Figure 4.1.8. And the right picture in Figure 4.1.8 demonstrates that the residual-based method has to use many degrees of freedom to get an accurate numerical result. While the MP-DWR method can obtain the numerical result satisfying the same precision with just a few degrees of freedom. This means that the MP-DWR method can construct a much more economical adapted mesh to capture quantities of interest precisely. Therefore, we can confirm the effectiveness of MP-DWR method in this convection-diffusion case.

4.2 Performance on acceleration

In this part, we will show one important advantage of the MP-DWR method in numerical simulations, i.e. the acceleration of simulations. Three classic DWR

approaches, i.e. h-approach, p-approach, and i-approach, are implemented during the experiments as comparisons. By comparing the CPU time consumption of each approach, we can test the acceleration capability of the MP-DWR method.

4.2.1 2D case

Above all, we consider the Poisson case as (27) with point-wise target functional J_p in (28). The exact solution is $u = 5.0 \times (1 - x_1^2)(1 - x_2^2) exp(1 - x_2^{-4})$ and the interested point is $\vec{x}_e = (0.2, 0.8)$. In this case, the DWR error indicators based on four different approaches (MP-DWR and three classic approaches) are generated from the same initial mesh with almost thirty thousands degrees of freedom. The process is repeated 100 times and the average CPU time of several operations in this process is recorded in Table 4.2.1. It can be seen that all approaches cost similar CPU time to obtain the primal solution. However, in order to generate the error indicator (including solving the dual problem and constructing the error indicator), four approaches cost quite different CPU time. First of all, h-approach has to spend extra time on remeshing. Besides that, h-approach and p-approach both use some time to building a new finite element space. On the contrary, the i-approach and MP-DWR method do not need to execute these operations of building new space. Moreover, since no more Dofs or mesh grid points are introduced, they cost much less time to build quadrature information and solve the linear system than the former two classic approaches. Therefore, the i-approach and MP-DWR method can save considerable CPU time compared with h- and p-approach. But then the iapproach has to spend some time on interpolation while constructing the error indicator. Due to such a difference, the MP-DWR method is slightly faster than the *i*-approach.

Operation	h-approach	p-approach	<i>i</i> -approach	MP-DWR
Build primal FEM space	8.915e0	8.274e0	7.825e0	8.154e0
Build Quadrature information	2.632e1	2.658e1	2.255e1	2.196e1
Solve Linear System	1.788e2	1.789e2	1.836e2	1.786e2
Remeshing	1.041e1			
Build dual FEM space	3.476e1	1.092e1		
Assemble Linear System	8.231e1	4.912e1	1.837e1	1.832e1
Solve Linear System	7.039e0	2.669e1	1.238e0	1.203e0
Construct indicator	2.999e1	2.934e1	3.420e1	2.815e1
Generate indicator	1.645e2	1.161e2	5.381e1	4.767e1
Total CPU time	3.785e2	3.298e2	2.678e2	2.564e2

Table 4.2.1 CPU time(seconds) of operations in the computation of Poisson case. The values are the average of 100 experimental results. The process of generating the indicator includes solving the dual problem and constructing the error indicator. For the *i*-approach, the CPU time for interpolation is included in the CPU time for the 'construct indicator' step.

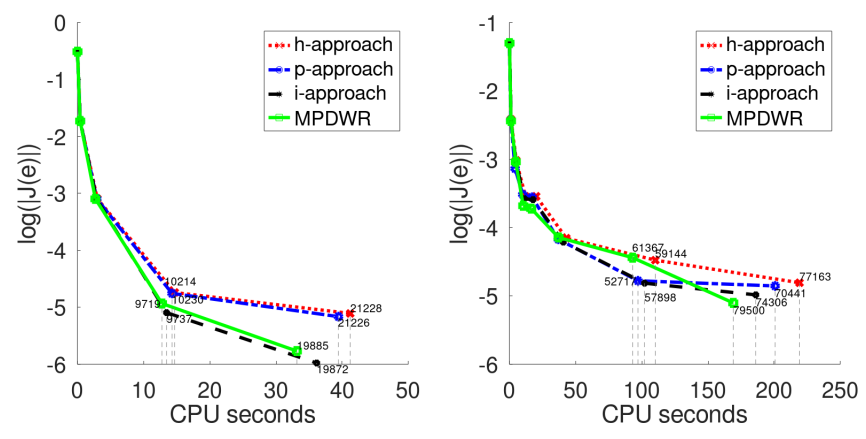


Fig. 4.2.1 The error and CPU time of the whole experiments based on MP-DWR and three classic DWR approaches. Left: with point-wise target functional. Right: with area target functional.

Furthermore, we implement the whole numerical simulation through each approach. The mesh adaptation is executed until the error tolerance is satisfied. The numerical results are shown in the left one of Table 4.2.1. Then we change the exact solution of Poisson case to $u_1 = (1 - x_1^2)(1 - x_2^2)\sin(4x_1)\sin(4x_2)$ with the area target functional $J_{\text{area}}(u)$ in (28). Similar simulations are implemented. The relationship between the error and whole CPU time for this case is shown in the right one of Figure 4.2.1.

In the left picture in Figure 4.2.1, it can be seen that the MP-DWR method and i-approach are much faster than h- and p-approach. The acceleration gets more obvious as the times of mesh adaptation increase. Then we focus on the comparison of MP-DWR and i-approach: the i-approach can control the error of the point-wise target functional better than MP-DWR method with a similar number of Dofs. But the CPU time of the MP-DWR method is always less than the i-approach. This suggests that the MP-DWR method may be less accurate but computationally fast compared to the i-method in this case. As for the right picture in Figure 4.2.1, it can be observed that the corresponding points of the MP-DWR method always stay at the most left position in each iteration step, which means that the MP-DWR method generally cost the least CPU time in simulations. When the iterations stop, although the MP-DWR method uses the most Dofs, the CPU time of the MP-DWR method is significantly less than the other three methods. This demonstrates that the MP-DWR method can be calculated faster than the three classical methods in this case.

4.2.2 3D case

Then we consider the Poisson equation in 3-dimensional with a target functional, which is given by:

$$J_G(u) = \int u d\vec{x}, \ \vec{x} = (x_1, x_2, x_3).$$
 (35)

The exact solution is given as the example in [15]:

$$u = (1 - x_1^2)^2 (1 - x_2^2)^2 (1 - x_3^2)^2 (64x_1^2 + 0.1)^{-1} (64x_3^2 + 0.1)^{-1}.$$
 (36)

The comparison of CPU time for the whole simulation based on the MP-DWR method and three classic approaches is similar to the 2D case in Figure 4.2.1. The MP-DWR method and *i*-approach demonstrate similar efficiency, and both of them are computed faster than the h- and p-approach. Then we mainly focus on the comparison of CPU time for generating the error indicator. Similar to the 2D case, we implement the four approaches to generate the error indicators from the same initial mesh (with almost 18000 Dofs), respectively. The CPU time for such a process is recorded in the Table 4.2.2. The values are the average of 100 experimental results. It can be observed that four approaches spend similar time on solving the primal problem. As for generating the error indicator (including solving the dual problem and constructing the error indicator), these approaches cost quite different CPU seconds. Compared to the i-approach, the MP-DWR method can save some CPU time during solving the dual problem since the involvement of singleprecision computations. Besides that, due to the increased number of elements and corresponding neighbors in the 3D case, higher-order interpolation takes more CPU time than in the 2D case. Consequently, the MP-DWR method can save much CPU time during constructing the indicator since it does not need the higher-interpolation operation. More importantly, compared to the h- and p-approach, the improvement in CPU time brought by the MP-DWR method is quite significant. The MP-DWR method can use the equivalent of about 15% of the time for the h-approach and about 30% of the time for the p-approach to generate the indicator. Based on that, we can demonstrate that the performance of the MP-DWR method in acceleration is quite considerable in the 3D case compared to the h- and p-approach. Therefore, the MP-DWR method can be more competitive in 3D numerical simulations.

4.3 Performance in eigenvalue problems

To extend the MP-DWR method into DFT (density functional theory), we spend some time on verifying its effectiveness in the eigenvalue problem, which is the critical part in the study of DFT. Consider the eigenvalue problem as follows. Seeking an eigenpair $(\lambda, u) \in \mathcal{C} \times H_0^1(\Omega)$ with

$$-\Delta u + \vec{\beta} \cdot \nabla u = \lambda u \text{ in } \Omega. \tag{37}$$

Operation	h-approach	p-approach	<i>i</i> -approach	MP-DWR
Build primal FEM space	3.086e0	3.048e0	2.825e0	3.196e0
Build Quadrature information	1.135e1	1.137e1	1.129e1	9.710e0
Solve Linear System	2.137e1	2.137e1	2.139e1	2.148e1
Remeshing	6.423e0			
Build dual FEM space	2.446e1	3.886e0		
Assemble Linear System	7.833e1	4.096e1	9.853e0	8.272e0
Solve Linear System	1.062e0	6.402e0	1.449e-1	1.447e-1
Construct indicator	9.956e0	1.033e1	2.157e1	9.691e0
Generate indicator	1.202e2	6.162e1	3.156e1	1.811e1
Total time	1.560e2	9.741e1	6.707e1	5.249e1

An MP-DWR method for h-adaptive finite element methods

Table 4.2.2 CPU time(seconds) of operations in 3-dimensional Poisson case. The values are the average of 100 experimental results. The process of generating the indicator includes solving the dual problem and constructing the error indicator. For the *i*-approach, the CPU time for interpolation is included in the CPU time for the 'construct indicator' step.

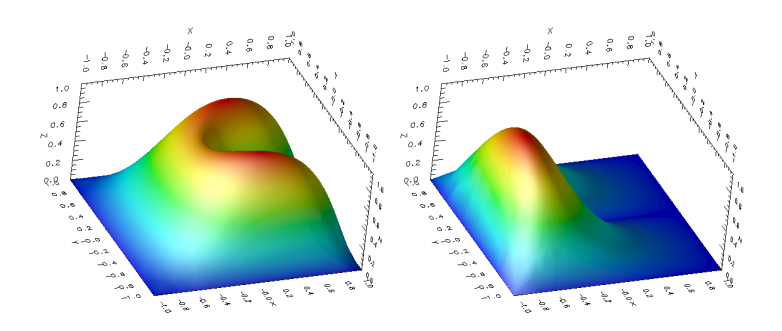


Fig. 4.3.1 Left: the plot figure of the primal solution. Right: dual solution.

In experiments, $\vec{\beta}$ is set as [3,0]. The computational domain is set as the slit area $\Omega_3 = ((-1,1) \times (-1,1)) \setminus ([0,1] \times \{0\})$. Following Appendix B, we can get the related error indicator for mesh adaptation. In the simulation of the MP-DWR method, we follow the framework of Algorithm 1, i.e. the primal solution and corresponding ρ_K are computed in double-precision. While the dual solution and ρ_K^* are computed in single-precision. Based on these, the error indicator η_λ^ω as (B18) can be computed. For comparison, the residual-based error indicator $\eta_\lambda^{\rm energy}$ as (B19) is also implemented. Figure 4.3.1 shows the numerical primal and dual solution. The residual of the smallest eigenvalue λ_1 over Dofs is shown in Figure 4.3.2. From Figure 4.3.2, it can be observed that, with the specified number of Dofs, the MPDWR method can get a more accurate result than the $\eta^{\rm energy}$ based method. This demonstrates that the MP-DWR method can deal with the interested eigenpair more efficiently. Consequently, it can be demonstrated that the MP-DWR method can still work in the eigenvalue problem. Based on these, it can be expected that the MP-DWR method can be applied to solve eigenvalue problems in DFT.

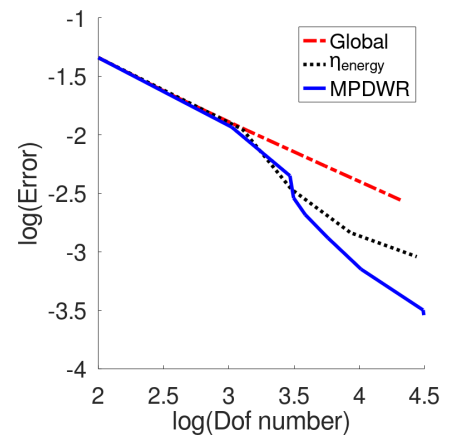


Fig. 4.3.2 The smallest eigenvalue errors over the number of Dofs.

4.4 The limit of MP-DWR method

In this part, we discuss a limit of the MP-DWR(FD) framework. In some numerical experiments, it is strange that MP-DWR(FD) becomes less effective with refining the mesh too many times. Consider the Poisson case with point-wise target functional in case 4.1.1. We solve the primal problem with single-precision and double-precision, respectively. The numerical results of the primal solutions are shown in Figure 4.4.1. It can be seen that when the mesh grids are dense enough, the residual in single-precision gets larger as the number of degrees of freedom increases, which is different from the residual in double-precision. With this unexpected phenomenon, it can not be expected that such an inaccurate primal solution in single-precision can construct a reliable DWR error indicator. One possible reason is that while we adapt the mesh several times, some area will gets quite dense and the minimal volume of elements will get very tiny. For reference, the minimal volumes of elements on the mesh grids in each iteration are shown in Table 4.4.1. When the minimal volume gets the level of 1.0e-6, the data in such an element can be close to the limit of single-precision so that the computations may demonstrate some unexpected phenomena causing the strange curve in Figure 4.4.1.

Table 4.4.1 The minimal volume of elements in adaptation

Adapt times	1	2	3	4	5
Minimal element volume	1.617e-2	1.010e-3	6.316 e- 05	4.34e-06	1.247e-06

Due to such a limit, we have to be careful about the data precision in numerical simulations while using the MP-DWR method.

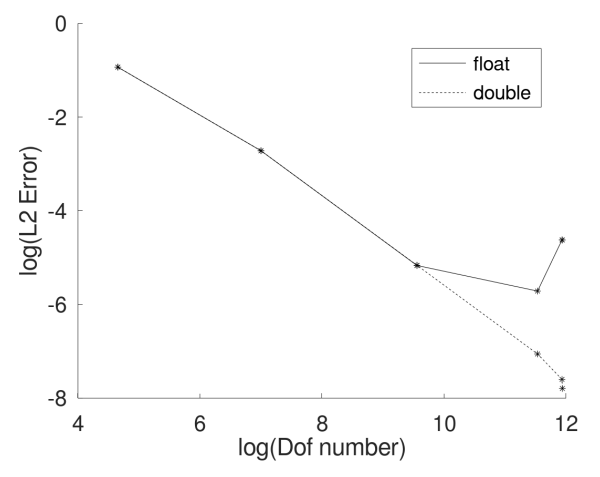


Fig. 4.4.1 Primal solutions computed in float and double precision.

Remark 3 Although there is a limit to the MP-DWR method, we propose a potential algorithm to make full use of the advantages of the MP-DWR method: First of all, we can compute the primal solution with half-precision and dual solution with single-precision, respectively. When the primal solution gets the limit of half-precision, we change the precision parameters in our programming to compute the primal with single-precision and dual solution with double-precision, respectively. In this way, we can make full use of the acceleration of the MP-DWR method to get a reliable numerical result. And such an algorithm can also be an efficient preconditioned approach.

5 Conclusion

To accelerate the process of obtaining dual solution in the DWR methods, we utilize the properties of precision formats and propose a novel DWR implementation based on multiple-precision named MP-DWR. Numerical experiments confirm the effectiveness of the novel approach. Memory storage savings can be expected due to the low-precision calculations involved. Furthermore, considerable reduction in CPU time compared with classic h- and p-approach is shown in simulations, which makes the MP-DWR method quite competitive. Compared with i-approach, the MP-DWR may lose some accuracy but it gains some acceleration in simulations, especially in the 3D case. By combining the MP-DWR method and i-approach, both of the accuracy and efficiency might be improved in simulations, which is our ongoing work. Although there is a limit to the MP-DWR method due to the property of precision formats in some situations, the substantial improvements in data storage and CPU time suggest that it is still an efficient method.

In addition, some more precise floating-point data type than double, such as __float128(long double), can be applied in the MP-DWR framework to

overcome the limit. Such an extension of the MP-DWR method will be implemented in our future study. In our previous work, applications of the h-adaptive method to computational fluid dynamics, micromagnetics, and density functional theory have been studied [26–30]. The introduction of the MP-DWR method into these applications to further improve the efficiency is also our future work. Besides that, the dual weighted residual method has been applied to many time-dependent problems [31–33], for which the MP-DWR is expected to be used to improve the computational efficiency.

Appendix A DWR method in the convection-diffusion equation

It has be noticed that, to solve (33), the bilinear form $a(\cdot,\cdot)$ is changed as

$$a(u,\varphi) = (\epsilon \nabla u, \nabla \varphi) + (\vec{\alpha} \cdot \nabla u, \varphi), \ \forall \varphi \in V.$$
 (A1)

Then by applying integration by parts, we can get the bilinear form of the dual problem, which is given by

$$a^*(z,\psi) = (\epsilon \nabla z, \nabla \psi) - (\vec{\alpha} \cdot \nabla z, \psi), \ \forall \psi \in V.$$
 (A2)

Based on this, the cell-wise error representation can be expressed as

$$J(u) - J(u_h) = \sum_{K \in \mathcal{T}_h} \{ (R_h, z)_K + \frac{1}{2} (r(\vec{n} \cdot \epsilon \nabla u_h), z)_{\partial_K} \}. \tag{A3}$$

With (A3), the error indicator for mesh adaptation can be obtained. We only consider the simple case here. More details and theories of the DWR method applied in convection-diffusion equations can be found in [15, 19].

Appendix B DWR method in the eigenvalue problem

To solve the (37), the corresponding bilinear form can be written as:

Finding eigenpairs
$$(\lambda, u) \in \mathcal{C} \times V$$
, $a(u, v) = \lambda b(u, v)$, $\forall v \in V$, (B4)

where $V := H_0^1(\Omega)$. The two bilinear forms $a(\cdot, \cdot)$ and $b(\cdot, \cdot)$ are given by:

$$a(u,v) := (\nabla u, \nabla v) + (\beta \cdot \nabla u, v), \tag{B5}$$

and

$$b(u,v) := (u,v). \tag{B6}$$

The corresponding dual eigenvalue problem can be defined as:

Finding dual eigenpairs
$$(\lambda_h^*, u_h^*) \in \mathcal{C} \times V_h$$
, (B7)

s.t.
$$a(v_h, u_h^*) = \overline{\lambda_h^*} b(v_h, u_h^*), \ \forall v_h \in V_h \subset V.$$
 (B8)

The eigenvalues $\lambda_{h,j}^*$ are related to the eigenvalues $\lambda_{h,j}$

$$\lambda_{h,j} = \overline{\lambda_{h,j}^*}, \ j = 1, \dots, dim(V_h).$$
 (B9)

By combining (B4) and (B7), the residual can be defined as

$$\rho(u_h, \lambda_h)(\cdot) = a(u_h, \cdot) - \lambda_h b(u_h, \cdot), \tag{B10}$$

and

$$\rho^*(u_h^*, \lambda_h^*)(\cdot) = a(\cdot, u_h^*) - \lambda_h^* b(\cdot, u_h^*). \tag{B11}$$

Then the error of $|\lambda - \lambda_h|$ can be bounded by the residuals:

$$|\lambda - \lambda_h| \le |\rho(u^* - \psi_h)| + |\rho^*(u - \phi_h)|, \ \forall \psi_h, \phi_h \in V_h.$$
 (B12)

On the mesh \mathcal{T} , the residual term in each linear piecewise element K can be expressed as

$$\rho_K := (\| -\Delta u + \vec{\beta} \cdot \nabla u - \lambda_h u_h \|_K^2 + h_K^{-1/2} \| r_h \|_{\partial_K}^2)^{1/2}, \tag{B13}$$

$$\rho_K^* := (\| -\Delta u + \vec{\beta} \cdot \nabla u - \overline{\lambda_h^* u_h^*} \|_K^2 + h_K^{-1/2} \|r_h^*\|_{\partial_K}^2)^{1/2}, \tag{B14}$$

where r_h and r_h^* represent the jump residual across the edge between two neighbor elements [15, 34]. With (B13), the residual satisfies the relationship as

$$|\rho(u^* - \psi_h) + \rho^*(u - \phi_h)| \le \sum_{K \in \mathcal{T}} {\{\rho_K \omega_K^* + \rho_K^* \omega_K\}},$$
 (B15)

with the weights ω_K and ω_K^* defined by

$$\omega_K := (\|u - \phi_h\|_K^2 + h_K^{1/2} \|u - \phi_h\|_{\partial K}^2)^{1/2}, \tag{B16}$$

$$\omega_K^* := (\|u^* - \psi_h\|_K^2 + h_K^{1/2} \|u^* - \psi_h\|_{\partial K}^2)^{1/2}$$
 (B17)

Based on (B12) and (B15), a dual weighted residual based error estimator on mesh \mathcal{T} can be given by

$$|\lambda - \lambda_h| \le \eta_\lambda^\omega := \sum_{K \in \mathcal{T}_h} \{ \rho_K \omega_K^* + \rho_K^* \omega_K \}.$$
 (B18)

And the "energy-norm-error-type" estimate can be given as

$$|\lambda - \lambda_h| \le \eta_{\lambda}^{\text{energy}} := c_{\lambda} \sum_{K \in \mathcal{T}_h} h_K^2 \{ \rho_K^2 + \rho_K^{*2} \}, \tag{B19}$$

with a constant c_{λ} growing linearly with $|\lambda|$. More details of the DWR method in eigenvalue problems can be found [15, 34, 35].

References

- [1] Babuška, I., Miller, A.: The post-processing approach in the finite element method—Part 1: calculation of displacements, stresses and other higher derivatives of the displacements. International Journal for numerical methods in engineering **20**(6), 1085–1109 (1984)
- [2] Babuška, I., Miller, A.: The post-processing approach in the finite element method—part 2: the calculation of stress intensity factors. International Journal for numerical methods in Engineering 20(6), 1111–1129 (1984)
- [3] Babuška, I., Miller, A.: A feedback finite element method with a posteriori error estimation: Part I. The finite element method and some basic properties of the a posteriori error estimator. Computer Methods in Applied Mechanics and Engineering 61(1), 1–40 (1987)
- [4] Eriksson, K., Johnson, C.: An adaptive finite element method for linear elliptic problems. Mathematics of Computation 50(182), 361–383 (1988)
- [5] Eriksson, K., Johnson, C.: Adaptive finite element methods for parabolic problems I: A linear model problem. SIAM Journal on Numerical Analysis **28**(1), 43–77 (1991)
- [6] Eriksson, K., Estep, D., Hansbo, P., Johnson, C.: Introduction to adaptive methods for differential equations. Acta numerica 4, 105–158 (1995)
- [7] Becker, R., Rannacher, R.: A feed-back approach to error control in finite element methods: Basic analysis and examples. East-West Journal of Numerical Mathematics 4 (1996)
- [8] Becker, R., Rannacher, R.: Weighted a Posteriori Error Control in FE Methods, (1996)
- [9] Becker, R., Rannacher, R.: An optimal control approach to a posteriori error estimation in finite element methods. Acta numerica 10, 1–102 (2001)
- [10] Rannacher, R.: Adaptive galerkin finite element methods for partial differential equations. Journal of Computational and Applied Mathematics

- **128**(1-2), 205–233 (2001)
- [11] Peraire, J., Patera, A.: Bounds for linear-functional outputs of coercive partial differential equations: local indicators and adaptive refinement. Studies in Applied Mechanics 47, 199–216 (1998)
- [12] Prudhomme, S., Oden, J.T.: On goal-oriented error estimation for elliptic problems: application to the control of pointwise errors. Computer Methods in Applied Mechanics and Engineering 176(1-4), 313–331 (1999)
- [13] Giles, M., Larson, M., Levenstam, M., Suli, E.: Adaptive error control for finite element approximations of the lift and drag coefficients in viscous flow (1997)
- [14] Giles, M.B., Süli, E.: Adjoint methods for PDEs: a posteriori error analysis and postprocessing by duality. Acta numerica 11, 145–236 (2002)
- [15] Bangerth, W., Rannacher, R.: Adaptive Finite Element Methods for Differential Equations, Springer Basel AG 2003
- [16] Rannacher, R.: Error Control in Finite Element Computations, pp. 247–278. Springer, Dordrecht (1999)
- [17] Bangerth, W., Geiger, M., Rannacher, R.: Adaptive galerkin finite element methods for the wave equation. Computational Methods in Applied Mathematics **10**(1), 3–48 (2010)
- [18] Kormann, K.: A time-space adaptive method for the Schrödinger Equation. Communications in Computational Physics **20**(1), 60–85 (2016)
- [19] Bruchhäuser, M.P., Schwegler, K., Bause, M.: Numerical study of goaloriented error control for stabilized finite element methods. In: Chemnitz Fine Element Symposium, pp. 85–106 (2017). Springer
- [20] Rabizadeh, E., Bagherzadeh, A.S., Anitescu, C., Alajlan, N., Rabczuk, T.: Pointwise dual weighted residual based goal-oriented a posteriori error estimation and adaptive mesh refinement in 2D/3D thermo-mechanical multifield problems. Computer Methods in Applied Mechanics and Engineering 359, 112666 (2020)
- [21] Avijit, D., Natesan, S.: An efficient DWR-type a posteriori error bound of SDFEM for singularly perturbed convection-diffusion PDEs. Journal of Scientific Computing **90**(2), 1–16 (2022)
- [22] Li, R.: On multi-mesh h-adaptive methods. Journal of Scientific Computing **24**(3), 321–341 (2005)

- An MP-DWR method for h-adaptive finite element methods
- [23] Verfürth, R.: A Posteriori Error Estimation Techniques for Finite Element Methods, OUP Oxford,2013
- [24] Richter, T., Wick, T.: Variational localizations of the dual weighted residual estimator. Journal of Computational and Applied Mathematics 279, 192–208 (2015)
- [25] Liu, C., Hu, G.: https://github.com/Mixed-DWR/MP-DWR_Example2.git
- [26] Bao, G., Hu, G., Liu, D.: An h-adaptive finite element solver for the calculations of the electronic structures. Journal of Computational Physics **231**(14), 4967–4979 (2012). https://doi.org/10.1016/j.jcp.2012.04.002
- [27] Bao, G., Hu, G., Liu, D.: Numerical solution of the Kohn-Sham equation by finite element methods with an adaptive mesh redistribution technique. Journal of Scientific Computing 55(2), 372–391 (2013)
- [28] Hu, G., Meng, X., Yi, N.: Adjoint-based an adaptive finite volume method for steady euler equations with non-oscillatory k-exact reconstruction. Computers & Fluids 139, 174–183 (2016)
- [29] Yang, L., Hu, G.: An adaptive finite element solver for demagnetization field calculation. Advances in Applied Mathematics and Mechanics (2019)
- [30] Meng, X., Hu, G.: A nurbs-enhanced finite volume method for steady euler equations with goal-oriented h-adaptivity. Communications in Computational Physics (2022)
- [31] Köcher, U., Bruchhäuser, M.P., Bause, M.: Efficient and scalable data structures and algorithms for goal-oriented adaptivity of space—time fem codes. SoftwareX 10, 100239 (2019)
- [32] Bruchhäuser, M.P., Schwegler, K., Bause, M.: Dual weighted residual based error control for nonstationary convection-dominated equations: Potential or ballast? Boundary and Interior Layers, Computational and Asymptotic Methods BAIL 2018, 1 (2020)
- [33] Sleeman, M.K., Yano, M.: Goal-oriented model reduction for parametrized time-dependent nonlinear partial differential equations. Computer Methods in Applied Mechanics and Engineering 388, 114206 (2022). https://doi.org/10.1016/j.cma.2021.114206
- [34] Gedicke, J.M.: On the numerical analysis of eigenvalue problems. PhD thesis, Humboldt-Universität zu Berlin, Mathematisch-Naturwissenschaftliche Fakultät II (2013). https://doi.org/10.18452/16841

[35] Heuveline, V., Rannacher, R.: A posteriori error control for finite element approximations of elliptic eigenvalue problems. Advances in Computational Mathematics **15**(1), 107–138 (2001)